Importance of interplane coupling on the magnetic phases of quasi-two-dimensional tantalites

2012 J. Phys.: Condens. Matter 24 256005

(http://iopscience.iop.org/0953-8984/24/25/256005)

J. Phys.: Condens. Matter **24** (2012) 256005 (8pp) doi:10.1088/0953-8984/24/25/256005

Importance of interplane coupling on the magnetic phases of quasi-two-dimensional tantalites

E G Santos[1,2], J B M da Cunha[1], O Isnard[2], C Lacroix[2] and M A Gusmão[1]

[1] Instituto de Física, Universidade Federal do Rio Grande do Sul, CP 15051, 91501-970 Porto Alegre, Brazil
[2] Institut Néel, CNRS/Université Joseph Fourier, BP 166, F-38042 Grenoble Cedex 9, France

E-mail: olivier.isnard@grenoble.cnrs.fr

Received 28 January 2012, in final form 4 April 2012
Published 28 May 2012
Online at stacks.iop.org/JPhysCM/24/256005

Abstract
We propose a three-dimensional model to describe magnetic interactions in a class of tantalite compounds of compositions $A_xA'_{1-x}Ta_2O_6$, with A, A′ = Fe, Co or Ni. Due to the quasi-two-dimensional nature of the magnetism in these compounds, experimental data have been previously interpreted using two-dimensional models. These are anisotropic Heisenberg models or Ising models and include competing exchange interactions from different neighbors. Taking into account all the relevant exchange terms, which include interplane interactions, we show that the latter allows us to understand the various low-temperature magnetic phases observed by neutron diffraction in this family of compounds. This is done by studying the eigenvalues of the exchange-interaction matrix in wavevector space for different sets of coupling parameters, of which those relative to in-plane interactions have been obtained from high-temperature series analysis of the magnetic susceptibility. This approach is rather general and the model presented here is directly applicable to isostructural compounds like ASb_2O_6.

(Some figures may appear in colour only in the online journal)

1. Introduction

The magnetic properties of a class of tantalite compounds, $A_xA'_{1-x}Ta_2O_6$ with A, A′ = Fe, Co or Ni have been the subject of extensive studies [1–10]. Their lattice structure is tetragonal, with two magnetic cations per unit cell, being classified in the $P4_2/mnm$ crystallographic group. Their magnetism is markedly two-dimensional, due to the presence of two planes of non-magnetic ions separating the magnetic ones, all of them stacked along the c axis. The magnetic ions are surrounded by distorted oxygen octahedra, with a short principal axis that yields an easy magnetic axis resulting from crystal-field single-ion anisotropy. These short octahedron axes change their orientation by 90° between the two magnetic positions in the cell, so that two neighboring magnetic planes present perpendicular anisotropy axes. These characteristics, as well as competition between nearest-neighbor (nn) and next-nearest-neighbor (nnn) exchange interactions, lead to a variety of non-Néel antiferromagnetic (AF) phases, observed by neutron diffraction at temperatures typically below 11 K.

Here we briefly review the main observations previously reported. $CoTa_2O_6$ presents a magnetic structure indexed by the propagation vectors $(\pm 1/4, 1/4, 1/4)$ [6–9], associated with magnetic ions at the corner and center of the structural unit cell. Following [10], we call this magnetic ordering AFC (C for Co). This phase is strongly unstable against Fe substitution, so that already slightly above 1% Fe it is replaced by a phase described by the propagation vectors $(\pm 1/4, 1/4, 0)$, which remains stable up to intermediate compositions, $x \simeq 0.46$. We call this structure AFI [10]. The iron-rich compounds of the $Fe_xCo_{1-x}Ta_2O_6$, for $x > 0.46$, present the magnetic structure of $FeTa_2O_6$, which we call AFF, and is described by the propagation vectors $(1/2, 0, 1/2)$ and $(0, 1/2, 1/2)$ [1–3]. The same magnetic structures are observed in the $Fe_xNi_{1-x}Ta_2O_6$ series, but a new ordering

appears for Ni-rich compounds, with propagation vectors $(\pm 1/4, 1/4, 1/2)$ [11–13]. which we will call AFN.

Both the low-dimensional character and the strong in-plane easy-axis anisotropy are very robust features of all these compounds. The magnetic moments always lie on the *ab* plane, alternating along the directions $[1, 1, 0]$ and $[1, \bar{1}, 0]$ from one plane to the next. These are the easy-axis directions, which follow the corresponding rotation of the oxygen octahedra in the trirutile structure.

Previous interpretations of the observed magnetic properties of these compounds were based on anisotropic Heisenberg models or on Ising models, in both cases involving competing exchange interactions among different neighbors [10, 14, 15]. The quasi-two-dimensional nature of these magnetic systems was confirmed by fittings of susceptibility data with high-temperature-series (HTS) expansions for planar versions of those models [10, 14]. Exchange parameters obtained from the fittings proved to be consistent with the magnetic orderings observed for the *ab* planes. However, as we have reviewed above, the magnetic structures obtained from neutron-diffraction experiments are three-dimensional, and some of them differ only along the *c* direction. This means that the interplane interactions, even though weak, do play a relevant role in stabilizing the low-temperature magnetic structures.

The aim of the present work is to complement our understanding of these systems by adding interplane exchange interactions to the above-mentioned models, and determining ranges of interplane coupling values that are compatible with each of the observed structures. Unfortunately, the existence of two magnetic ions per unit cell of the crystal structure and the need to take into account competing interactions among first- and second-nearest neighbors in each direction make the task of extending the HTS treatment extremely difficult. For this reason, we have chosen a simpler approach, essentially based on the ability of the mean-field approximation to capture the correct periodicity of a magnetic structure. For a single spin per unit cell, and isotropic exchange of the form $J_{ij}\mathbf{S}_i \cdot \mathbf{S}_j$, the Fourier components of the mean-field paramagnetic susceptibility are given by

$$\chi(\mathbf{q}) = \frac{C}{T - 2CJ(\mathbf{q})}, \tag{1}$$

where C is the Curie constant, T is the temperature and $J(\mathbf{q})$ denotes the Fourier transform of the exchange couplings J_{ij}. Thus, the $\mathbf{q}$-dependent susceptibility that diverges at the highest temperature (T_N) corresponds to a wavevector $\mathbf{Q}$ such that $J(\mathbf{Q}) \equiv \max[J(\mathbf{q})]$. This is the wavevector that describes the ordered magnetic structure, i.e. the Fourier component $\mathbf{M}(\mathbf{Q})$ of the magnetization is non-zero below T_N in the absence of an applied field.

When there are more than one magnetic atoms per unit cell, and/or in the presence of anisotropy, the exchange constants define an exchange matrix for each wavevector. If we have r magnetic atoms per unit cell and in the anisotropic case, we end up with a square matrix of dimension $3r$, since the three spin components are not equivalent. The largest eigenvalue of this matrix, $\lambda(\mathbf{Q})$, gives the $\mathbf{Q}$ vector corresponding to the magnetic order that is stabilized at the transition, while the corresponding eigenvector $\mathbf{v}(\mathbf{Q})$ provides information about the arrangement of magnetic moments within the unit cell. This approach was employed in various studies of magnetic ordering in solids a few decades ago [16–20] and presented in a systematic form by Bertaut [21, 22]. Here we will use it in connection with a generalization of previously proposed models for the $A_xA'_{1-x}Ta_2O_6$ system, studying the existence and stability of the various magnetic phases described above.

2. Three-dimensional model

Based on the planar models previously developed [10, 14, 15], we will construct an anisotropic Heisenberg model with first- and second-neighbor exchange interactions both in the *ab* plane and between planes. We start by noticing that the two families of magnetic planes correspond to the two structural sublattices of the $P4_2/mnm$ structure, which we will label α and β. Since the anisotropy axes of α and β sites are perpendicular, we will define the spin coordinates so that the x and y axes correspond to the lattice directions [110] and $[\bar{1}10]$, respectively, while the z axis lies along [001].

We write the Hamiltonian separating the planar (pl) and interplane (ip) contributions:

$$\mathcal{H} = \mathcal{H}^{\alpha}_{\mathrm{pl}} + \mathcal{H}^{\beta}_{\mathrm{pl}} + \mathcal{H}_{\mathrm{ip}}, \tag{2}$$

where

$$\mathcal{H}^{\alpha}_{\mathrm{pl}} = -2J_1 \sum_{\langle ij\rangle}^{\mathrm{nn}} \mathbf{S}_{i\alpha} \cdot \mathbf{S}_{j\alpha} - 2J_2 \sum_{\langle ij\rangle}^{[110]} \mathbf{S}_{i\alpha} \cdot \mathbf{S}_{j\alpha} - 2J'_2 \sum_{\langle ij\rangle}^{[\bar{1}10]} \mathbf{S}_{i\alpha} \cdot \mathbf{S}_{j\alpha} - D \sum_i (S^x_{i\alpha})^2, \tag{3}$$

$$\mathcal{H}^{\beta}_{\mathrm{pl}} = -2J_1 \sum_{\langle ij\rangle}^{\mathrm{nn}} \mathbf{S}_{i\beta} \cdot \mathbf{S}_{j\beta} - 2J'_2 \sum_{\langle ij\rangle}^{[110]} \mathbf{S}_{i\beta} \cdot \mathbf{S}_{j\beta} - 2J_2 \sum_{\langle ij\rangle}^{[\bar{1}10]} \mathbf{S}_{i\beta} \cdot \mathbf{S}_{j\beta} - D \sum_i (S^y_{i\beta})^2, \tag{4}$$

$$\mathcal{H}_{\mathrm{ip}} = -2J_3 \sum_{\langle ij\rangle}^{\mathrm{nn}} \mathbf{S}_{i\alpha} \cdot \mathbf{S}_{j\beta} - 2J'_3 \sum_{\langle ij\rangle}^{\mathrm{nnn}} \mathbf{S}_{i\alpha} \cdot \mathbf{S}_{j\beta} - 2J_4 \sum_{\langle ij\rangle}^{[001]} \mathbf{S}_{i\alpha} \cdot \mathbf{S}_{j\alpha} - 2J_4 \sum_{\langle ij\rangle}^{[001]} \mathbf{S}_{i\beta} \cdot \mathbf{S}_{j\beta}. \tag{5}$$

For a better visualization of the various exchange couplings, they are schematically depicted in figure 1. It should be noticed that the interplane Hamiltonian contains inter-sublattice terms (with J_3 and J'_3) as well as intra-sublattice terms (with J_4). The notation $\langle ij\rangle$ stands for the pair of sites that are nearest along the direction specified on the sum, except for nearest neighbors in a plane (J_1 terms), and for the inter-sublattice sums, where we refer to nearest neighbors (nn) and next-nearest neighbors (nnn) in adjacent planes.

We can view the anisotropy as a 'local exchange' coupling involving a single spin component. With this, the

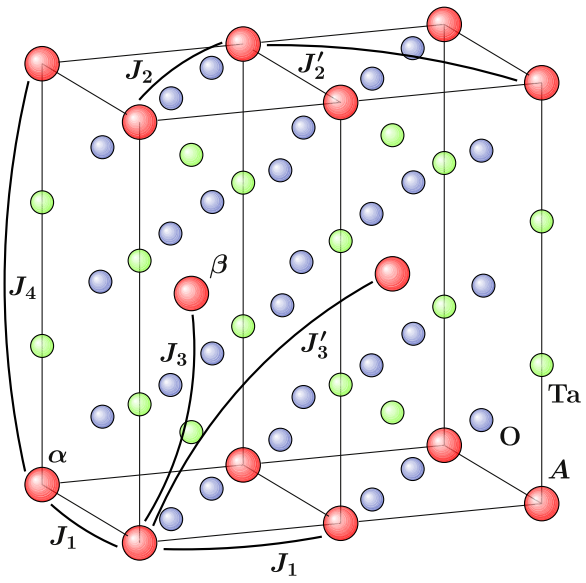

Figure 1. Two unit cells of the ATa_2O_6 structure, showing the magnetic sites α and β, as well as representative pairs of magnetic ions interacting via the exchange couplings appearing in (3)–(5).

Hamiltonian can be written in a compact form:

$$\mathcal{H} = \sum_{ij} \sum_{\alpha\beta} \sum_{\mu\nu} S_{i\alpha}^{\mu} J_{ij}^{\alpha\mu,\beta\nu} S_{j\beta}^{\nu}, \tag{6}$$

where the sum over lattice sites now includes the case $i = j$ (anisotropy) and all the sites that are connected by exchange interactions. After Fourier-transforming, we can arrange the exchange matrix in the form

$$\mathcal{J}(\mathbf{k}) = \begin{bmatrix} \eta(\mathbf{k}) & \delta(\mathbf{k}) & 0 & 0 & 0 & 0 \\ \delta(\mathbf{k}) & \gamma_0(\mathbf{k}) & 0 & 0 & 0 & 0 \\ 0 & 0 & \eta_0(\mathbf{k}) & \delta(\mathbf{k}) & 0 & 0 \\ 0 & 0 & \delta(\mathbf{k}) & \gamma(\mathbf{k}) & 0 & 0 \\ 0 & 0 & 0 & 0 & \eta_0(\mathbf{k}) & \delta(\mathbf{k}) \\ 0 & 0 & 0 & 0 & \delta(\mathbf{k}) & \gamma_0(\mathbf{k}) \end{bmatrix}, \tag{7}$$

where each of the 2×2 blocks corresponds to a given spin component (in the order x, y, z along the diagonal) for both magnetic sites, and the matrix elements can be written as follows:

$$\begin{aligned} \eta_0(\mathbf{k}) &= 2J_1[\cos k_a + \cos k_b] + 2J_2 \cos(k_a + k_b) \\ &\quad + 2J_2' \cos(k_a - k_b) + 2J_4 \cos k_c, \qquad (8) \\ \eta(\mathbf{k}) &= \eta_0(\mathbf{k}) + D, \qquad (9) \\ \gamma_0(\mathbf{k}) &= 2J_1[\cos k_a + \cos k_b] + 2J_2 \cos(k_a - k_b) \\ &\quad + 2J_2' \cos(k_a + k_b) + 2J_4 \cos k_c, \qquad (10) \\ \gamma(\mathbf{k}) &= \gamma_0(\mathbf{k}) + D, \qquad (11) \\ \delta(\mathbf{k}) &= 8 \cos(k_a/2) \cos(k_b/2) \cos(k_c/2) \\ &\quad \times \{J_3 - 2J_3'[3 - 2\cos^2(k_a/2) - 2\cos^2(k_b/2)]\}, \qquad (12) \end{aligned}$$

where we defined the dimensionless wavevector components $k_a \equiv \mathbf{k}\cdot\mathbf{a}$, $k_b \equiv \mathbf{k}\cdot\mathbf{b}$, $k_c \equiv \mathbf{k}\cdot\mathbf{c}$, in terms of the usual orthogonal primitive lattice vectors of the tetragonal lattice, for which we have $|\mathbf{a}| = |\mathbf{b}| \neq |\mathbf{c}|$. With this notation, the $\mathbf{Q}$ vector of a given magnetic structure, i.e. the $\mathbf{k}$ vector corresponding to the global maximum of all the eigenvalues, differs by a factor of 2π from the usual propagation vector of neutron-diffraction analysis.

The blocks of $\mathcal{J}(\mathbf{k})$ can be diagonalized separately, so that the six eigenvalues can be written as

$$\begin{aligned} \lambda_{1\pm}(\mathbf{k}) &= \tfrac{1}{2}\{[\eta(\mathbf{k}) + \gamma_0(\mathbf{k})] \\ &\quad \pm \sqrt{[\eta(\mathbf{k}) - \gamma_0(\mathbf{k})]^2 + 4\delta^2(\mathbf{k})}\}, \\ \lambda_{2\pm}(\mathbf{k}) &= \tfrac{1}{2}\{[\eta_0(\mathbf{k}) + \gamma(\mathbf{k})] \\ &\quad \pm \sqrt{[\eta_0(\mathbf{k}) - \gamma(\mathbf{k})]^2 + 4\delta^2(\mathbf{k})}\}, \\ \lambda_{3\pm}(\mathbf{k}) &= \tfrac{1}{2}\{[\eta_0(\mathbf{k}) + \gamma_0(\mathbf{k})] \\ &\quad \pm \sqrt{[\eta_0(\mathbf{k}) - \gamma_0(\mathbf{k})]^2 + 4\delta^2(\mathbf{k})}\}. \end{aligned} \tag{13}$$

The corresponding normalized eigenvectors are

$$\begin{aligned} \mathbf{v}_{1+}(\mathbf{k}) &= \frac{1}{\xi_1(\mathbf{k})}(1\ , \phi_1(\mathbf{k}), 0, 0, 0, 0), \\ \mathbf{v}_{1-}(\mathbf{k}) &= \frac{1}{\xi_1(\mathbf{k})}(-\phi_1(\mathbf{k}), 1, 0, 0, 0, 0), \end{aligned} \tag{14}$$

and similarly for $\mathbf{v}_{2\pm}(\mathbf{k})$ and $\mathbf{v}_{3\pm}(\mathbf{k})$ in terms of $\xi_2(\mathbf{k})$, $\xi_3(\mathbf{k})$, $\phi_2(\mathbf{k})$, and $\phi_3(\mathbf{k})$, at the respective positions in the four-component vectors, with the definitions

$$\begin{aligned} \phi_1(\mathbf{k}) &= [\lambda_{1+}(\mathbf{k}) - \eta(\mathbf{k})]/\delta(\mathbf{k}) \\ &= -[\lambda_{1-}(\mathbf{k}) - \gamma_0(\mathbf{k})]/\delta(\mathbf{k}), \\ \phi_2(\mathbf{k}) &= [\lambda_{2+}(\mathbf{k}) - \eta_0(\mathbf{k})]/\delta(\mathbf{k}) \\ &= -[\lambda_{2-}(\mathbf{k}) - \gamma(\mathbf{k})]/\delta(\mathbf{k}), \\ \phi_3(\mathbf{k}) &= [\lambda_{3+}(\mathbf{k}) - \eta_0(\mathbf{k})]/\delta(\mathbf{k}) \\ &= -[\lambda_{3-}(\mathbf{k}) - \gamma_0(\mathbf{k})]/\delta(\mathbf{k}), \\ \xi_l(\mathbf{k}) &= \sqrt{1 + \phi_l^2(\mathbf{k})} \qquad (l = 1, 2, 3). \end{aligned} \tag{15}$$

In the case of strong anisotropy, since only $\gamma(\mathbf{k})$ and $\eta(\mathbf{k})$ contain D, the maximum eigenvalue can only be $\lambda_{1+}(\mathbf{k})$ or $\lambda_{2+}(\mathbf{k})$. Inspecting equation (8)–(13), one can see that these latter eigenvalues are equivalent to each other upon exchanging $J_2 \leftrightarrow J_2'$, with the accompanying exchange of x and y components of the eigenvectors $\mathbf{v}_{1\pm}$ and $\mathbf{v}_{2\pm}$. This corresponds to moving between the two families of magnetic planes that differ by a 90° rotation of the anisotropy axis. Due to this equivalence, we choose to focus on $\lambda_{1+}(\mathbf{k})$, for which the anisotropy axis lies along the direction $[1, 1, 0]$, i.e. α planes in the notation of (3)–(5). Obviously, the complete solution must combine both $\lambda_{1+}(\mathbf{k})$ and $\lambda_{2+}(\mathbf{k})$, which determine respectively the x and y components of the magnetization.

3. Analysis of the magnetic structures

With the model established and the exchange matrix determined, we now apply the mean-field Bertaut's method to analyze the observed magnetic structures in $A_xA'_{1-x}Ta_2O_6$ compounds. Since there are many coupling parameters and, in principle, the whole first Brillouin zone to explore, we will choose the following strategic approach. Given that the

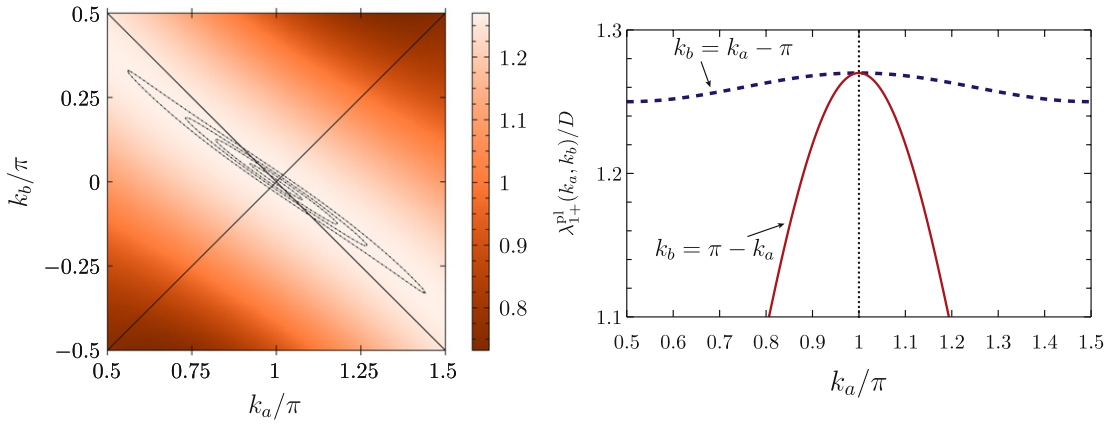

Figure 2. Left: color map and some contours of the eigenvalue $\lambda^{\rm pl}_{1+}(k_a, k_b)$ for decoupled planes. The color scale indicates values measured in units of the anisotropy constant, which has been chosen as $D = 10$ K for the plots. The exchange parameters are $J_1 = 0.48$ K, $J_2 = -1.3$ K and $J_2' = -0.05$ K, previously obtained [10] for $Fe_xCo_{1-x}Ta_2O_6$ with $x \simeq 0.6$. Right: plot along two crossing lines near the maximum, confirming its position at $(\pi, 0)$.

paramagnetic phase of the entire family of compounds was well described by a planar model with strong anisotropy (Ising model) [10], we will start by checking whether the exchange parameters determined by fittings of the susceptibility with the planar model actually correspond to maxima of the eigenvalue $\lambda_{1+}(\mathbf{k})$ for decoupled planes. We will then turn on interplane coupling and study the maxima also along the transverse direction. This will be particularly important to compare the AFC, AFI and AFN phases, which have the same planar structures but different ordering along the c axis.

3.1. Magnetic structures for decoupled planes

As we mentioned before, the relevant eigenvalue of our exchange-coupling matrix is $\lambda_{1+}(\mathbf{k})$. When the interplane exchange constants J_3, J_3' and J_4 are set to zero in (8)–(13), it assumes the form

$$\lambda^{\rm pl}_{1+}(k_a, k_b) = D + 2J_1(\cos k_a + \cos k_b) + 2J_2 \cos(k_a + k_b) + 2J_2' \cos(k_a - k_b). \quad (16)$$

Equating to zero the derivatives of $\lambda^{\rm pl}_{1+}(k_a, k_b)$ with respect to its arguments, we can sum and subtract the resulting equations to obtain

$$\begin{aligned} J_1(\sin k_a + \sin k_b) + 2J_2 \sin(k_a + k_b) = 0, \\ J_1(\sin k_a - \sin k_b) + 2J_2' \sin(k_a - k_b) = 0. \end{aligned} \quad (17)$$

One can easily see that these equations have solutions for $(0, 0)$ (ferromagnetic), (π, π) (simple Néel AF) and $(0, \pi)$ or $(\pi, 0)$, the latter corresponding to the in-plane part of the AFF structure discussed in section 1. Apart from these, we have 'non-trivial' solutions for $k_a = k_b \equiv \kappa$, with

$$\cos\kappa = -\frac{J_1}{2J_2}, \quad (18)$$

and for $k_a = -k_b \equiv \kappa'$, with

$$\cos\kappa' = -\frac{J_1}{2J_2'}, \quad (19)$$

for $|J_1| < 2|J_2|$ or $|J_1| < 2|J_2'|$, respectively. These last two solutions differ by a 90° rotation of the wavevector and by the interchange of J_2 and J_2'. Therefore, when the solution (κ, κ) is stable in the α planes, the solution $(-\kappa, \kappa)$ will be stable in the β planes, since the latter corresponds to substituting J_2 for J_2' in (19), as discussed after (15).

When more than one maximum exist in $\mathbf{k}$ space, the actual solution corresponds to the highest one, which will depend on the specific values of the model parameters. Here the anisotropy parameter D plays an important role, even though it is not present in the equations obtained from derivatives of the eigenvalues.

As a check of consistency, we take from [10] two sets of values of exchange constants, determined with the planar model, for two representative compositions in the $Fe_xCo_{1-x}Ta_2O_6$ series. Following the common usage, we quote exchange constants in units of temperature, omitting the Boltzmann constant factor. For a Fe-rich sample near $x = 0.6$ we have $J_1 = 0.48$ K, $J_2 = -1.3$ K and $J_2' = -0.05$ K. For a Co-rich sample near the transition between the AFC and AFI phases ($x \lesssim 0.2$) the values are $J_1 = -0.45$ K, $J_2 = -2.8$ K and $J_2' = 0.3$ K. Utilizing these exchange values in the present model, we choose a large anisotropy ($D = 10$ K) to approach the Ising limit and take the interplane couplings as zero in this first check. Although one should expect different values of D for different compositions, we used the same reference value for all the numerical results. The role of the anisotropy is essentially to select $\lambda_{1+}(\mathbf{k})$ as the relevant eigenvalue and to set the scale of its values, without significant effect on the positions of the maxima.

On the left panel of figure 2 we show an intensity plot and some contours of $\lambda^{\rm pl}_{1+}(k_a, k_b)$ for the Fe-rich case. Even though the maximum is very extended along a ridge line nearly perpendicular to the direction $k_b = k_a$, its location at the point $(\pi, 0)$ is clearly seen. To confirm this, the panel on the right figure 2 shows that the point $(\pi, 0)$ is a maximum along both lines. The corresponding plots for the Co-rich case are shown in figure 3, where the position of the maximum is consistent with the κ value calculated from (18).

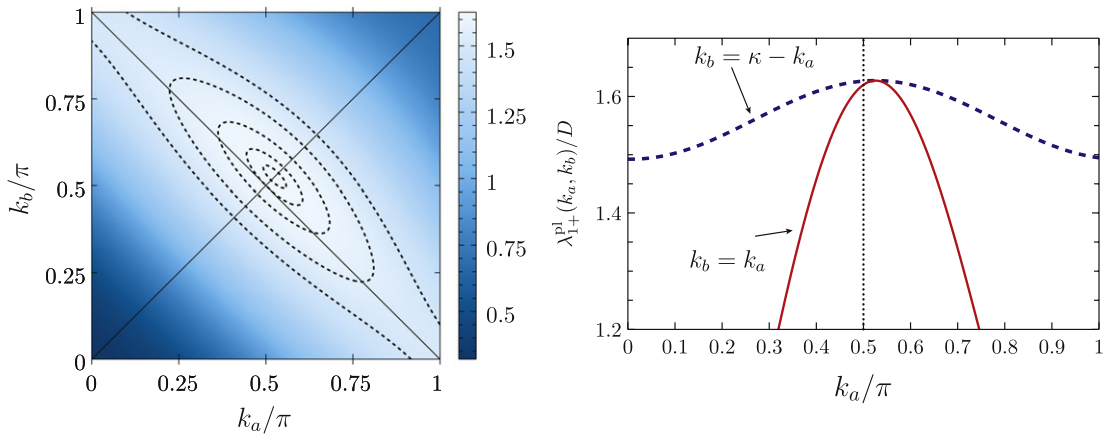

Figure 3. Plots like those shown in figure 2, but now for the parameter values $J_1 = -0.45$ K, $J_2 = -2.8$ K and $J_2' = 0.3$ K, obtained [10] for $Fe_xCo_{1-x}Ta_2O_6$ with $x \lesssim 0.2$. The value of κ is determined using (18). Notice that the maximum is at an incommensurate wavevector, slightly displaced from $(\pi/2, \pi/2)$, the ordering vector observed by neutron diffraction.

Notice that (κ, κ) is an incommensurate wavevector ($\kappa \simeq 0.52\,\pi$), although it is close to $(\pi/2, \pi/2)$, which corresponds to the *ab* plane components of the propagation vectors for both the AFC and the AFI magnetic structures. Inspecting the eigenvectors $\mathbf{v}_{1+}(\mathbf{k})$ and $\mathbf{v}_{2+}(\mathbf{k})$ (equations (14) and (15)), we can easily see that each spin lies essentially along the local anisotropy axis when D is large and the planes are weakly coupled. Thus if $\mathbf{Q}$ is incommensurate, the value of the local moment $|\langle \mathbf{S}_i \rangle|$ is modulated. This could be a possible state just below T_N, but at low temperatures the magnetic moments cannot be modulated because $|\langle \mathbf{S}_i \rangle| \to S$, which implies that the magnetic structure becomes commensurate. With the parameters considered above, the incommensurate structure is very close to the commensurate one with $(\pi/2, \pi/2)$, which becomes the stable structure. As the temperature rises towards T_N, since the average values of the spins no longer need to be maximal, one could see commensurate–incommensurate transitions. In this sense, our model is qualitatively similar to the well-studied ANNNI model [23], which shows a sequence of such transitions generating the famous devil's staircase.

3.2. *Effect of interplane coupling*

Following our strategy, we now study the stability of the in-plane solutions shown in figures 2 and 3 in the presence of interplane coupling, also determining which periodicity is favored in the c direction.

Keeping in mind that we are analyzing the eigenvalue $\lambda_{1+}(\mathbf{k})$, given by the first line of (13), we can see from (12) that the effect of the nearest plane (inter-sublattice coupling) goes to zero if any of the wavevector components is equal to π. In this case, $k_c = \pi$ is favored for $J_4 < 0$, as shown by (8). This is consistent with the experimental results for Fe-rich compounds in the $Fe_xCo_{1-x}Ta_2O_6$ series, for which the AFF structure presented in section 1 was observed, its propagation vector $(1/2, 0, 1/2)$ corresponding to $(k_a, k_b, k_c) = (\pi, 0, \pi)$.

Even though the inter-sublattice couplings J_3 and J_3' do not affect the value of $\lambda_{1+}(\pi, 0, \pi)$, we must check the stability of this structure upon increasing values of these parameters, since other solutions could yield a higher eigenvalue. Since the other possible maximum for decoupled planes occurs at $(k_a, k_b) \simeq (\pi/2, \pi/2)$, we must study how it changes with interplane coupling. From (12) we see that the inter-sublattice couplings do contribute in this case, predominantly in the combination $J_3 - 2J_3'$, so that they maximize $\delta(\mathbf{k})$ when their signs are opposite. We verified numerically that the AFF structure is stable if all the interplane couplings are weak, i.e. if their absolute values are one order of magnitude smaller than those of the dominant in-plane interactions J_1 and J_2. However, if J_3 and/or $|J_3'|$ become comparable to $|J_2|$, the maximum near $(\pi/2, \pi/2, 0)$ becomes the dominant one. This is shown in figure 4, where we plot the variation of the $\lambda_{1+}(\mathbf{k})$ as a function of k_c for (k_a, k_b) fixed at the observed maxima for decoupled planes. In the left panel of figure 4 the global maximum is at $(\pi, 0, \pi)$, corresponding to the AFF magnetic structure. Increasing the combination J_3–$2J_3'$ (in this case, by a small increase of $|J_3'|$), we see in the right panel that the global maximum becomes the one at $(\pi/2, \pi/2, 0)$, which characterizes the AFI structure, as discussed in section 1. The fact that this structure is not observed experimentally for Fe-rich compounds is consistent with the above analysis, as one would need very strong interplane interactions to stabilize it.

We now repeat this analysis using in-plane exchange constants obtained for Co-rich samples of the same series [10], for which a transition between the AFC and AFI structures (see section 1) was observed as the composition changed. First of all, we observed that the in-plane position of the maximum near $(\pi/2, \pi/2)$, shown in figure 3, is very stable against interplane coupling. We can understand this if we notice that the square root containing $\delta(\mathbf{k})$ in the expression for $\lambda_{1+}(\mathbf{k})$ (see (13)) is dominated by the anisotropy D and by the strongest in-plane exchange constant J_2. The two competing structures in the Co-rich region of compositions, AFC and AFI, differ only by their periodicity along c, as we have $k_c = \pi/2$ in AFC and $k_c = 0$ in AFI. For reasonable values of J_3 and J_3', i.e. substantially smaller than the in-plane couplings, the choice between these two magnetic

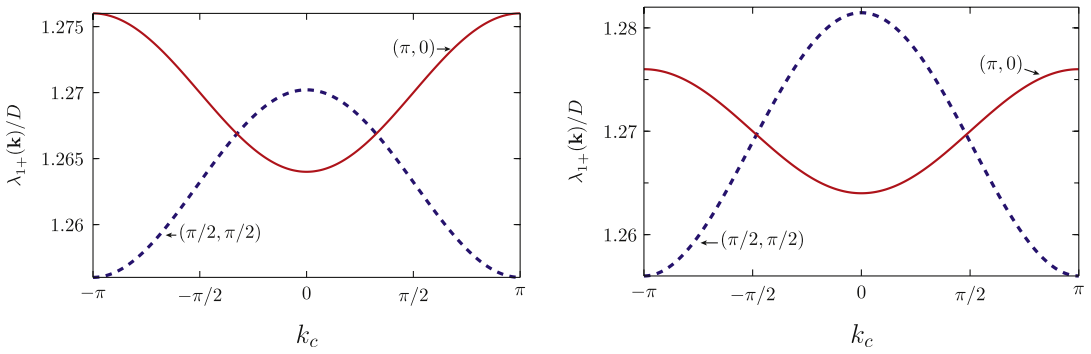

Figure 4. Behavior of the eigenvalue $\lambda_{1+}(\mathbf{k})$ as a function of k_c for (k_a, k_b) fixed at the two positions of the maxima obtained for decoupled planes. The values of the exchange parameters used in the left panel are $J_1 = 0.48$ K, $J_2 = -1.3$ K, $J_2' = -0.05$ K, $J_3 = 0.30$ K, $J_3' = -0.10$ and $J_4 = -0.05$ K, for which the global maximum is seen to be at $(\pi, 0, \pi)$. The only difference in the right panel is that the absolute value $|J_3'|$ increases from 0.10 to 0.15. Now the previously secondary maximum at $(\pi/2, \pi/2, 0)$ becomes the global one.

structures is made by J_4, which does not contribute to AFC but favors AFI when assuming a positive value, as can be checked through (8).

As we mentioned before, besides the AFC and AFI magnetic structures, the AFN phase appearing in the $Fe_xNi_{1-x}Ta_2O_6$ series also shows the same in-plane spin pattern, but with $k_c = \pi$. For this reason, the stability of the AFC structure presents some subtleties that deserve further analysis. From (8)–(13), we can write an equation for $\lambda_{1+}(\mathbf{k})$ as a function of k_c with fixed $k_a = k_b = \pi/2$:

$$\lambda_{1+}\left(\frac{\pi}{2}, \frac{\pi}{2}, k_c\right) = \tfrac{1}{2}[D + \sqrt{[D - 4(J_2 - J_2')]^2 + 64(J_3 - 2J_3')^2\cos^2(k_c/2)}] + 2J_4 \cos k_c. \tag{20}$$

Now, replacing k_c by 0, $\pi/2$ and π, we obtain, respectively:

$$\begin{aligned}
&\lambda_{1+}\left(\frac{\pi}{2}, \frac{\pi}{2}, 0\right) \\
&\quad = \tfrac{1}{2}[D + \sqrt{[D - 4(J_2 - J_2')]^2 + 64(J_3 - 2J_3')^2}] \\
&\quad + 2J_4, \\
&\lambda_{1+}\left(\frac{\pi}{2}, \frac{\pi}{2}, \frac{\pi}{2}\right) \\
&\quad = \tfrac{1}{2}[D + \sqrt{[D - 4(J_2 - J_2')]^2 + 32(J_3 - 2J_3')^2}], \\
&\lambda_{1+}\left(\frac{\pi}{2}, \frac{\pi}{2}, \pi\right) = D - 2(J_2 - J_2') - 2J_4.
\end{aligned} \tag{21}$$

With the correspondences $(\frac{\pi}{2}, \frac{\pi}{2}, 0) \rightarrow$ AFI, $(\frac{\pi}{2}, \frac{\pi}{2}, \frac{\pi}{2}) \rightarrow$ AFC, and $(\frac{\pi}{2}, \frac{\pi}{2}, \pi) \rightarrow$ AFN, we can rewrite these equations as

$$\begin{aligned}
\lambda_{1+}^{\mathrm{AFI}} &= \lambda_0 + \frac{1}{2}\tilde{D}\left[\sqrt{1 + 4\left(\frac{\delta_3}{\tilde{D}}\right)^2} - 1\right] + 2J_4, \\
\lambda_{1+}^{\mathrm{AFC}} &= \lambda_0 + \frac{1}{2}\tilde{D}\left[\sqrt{1 + 2\left(\frac{\delta_3}{\tilde{D}}\right)^2} - 1\right], \\
\lambda_{1+}^{\mathrm{AFN}} &= \lambda_0 - 2J_4,
\end{aligned} \tag{22}$$

where $\lambda_0 \equiv D - 2(J_2 - J_2')$ is the eigenvalue in the absence of interplane coupling, $\tilde{D} \equiv D - 4(J_2 - J_2')$ and $\delta_3 \equiv 4(J_3 - 2J_3')$. It is easy to see that $J_4 > 0$ stabilizes the AFI structure, while $J_4 < 0$ tends to favor AFN, but it is not clear what happens if J_4 is very small and negative, since even the AFI phase can be stable in this limit. Expanding the square roots up to second order, we obtain that the AFC phase is stable if J_4 is negative and its absolute value satisfies the conditions

$$\frac{1}{2}\frac{\delta_3^2}{\tilde{D}} - \frac{3}{4}\frac{\delta_3^4}{\tilde{D}^3} < 2|J_4| < \frac{1}{2}\frac{\delta_3^2}{\tilde{D}} - \frac{1}{4}\frac{\delta_3^4}{\tilde{D}^3}. \tag{23}$$

This narrow stability region of the AFC phase is consistent with the experimental observation that it is suppressed in favor of AFI at about 1% substitution of Fe for Co.

Summarizing the above discussion, we can highlight the following points concerning the observed magnetic phases in the $Fe_xCo_{1-x}Ta_2O_6$ and $Fe_xNi_{1-x}Ta_2O_6$ series.

(i) The AFF structure, with propagation vector (1/2, 0, 1/2), which is observed in Fe-rich compounds of the $Fe_xCo_{1-x}Ta_2O_6$ series, is essentially stabilized by the intra-plane exchange couplings as obtained from fittings of the susceptibility [10] and by an intra-sublattice interplane exchange $J_4 < 0$. This structure is robust against variations of the exchange interactions between nearest planes, J_3 and J_3', provided they are weak in comparison with the dominant in-plane coupling J_2.

(ii) The AFC and AFI structures, respectively with propagation vectors (1/4, 1/4, 1/4) and (1/4, 1/4, 0), present the same spin pattern on the *ab* plane, which differs from that of the AFF structure due to important changes observed in the in-plane exchange constants [10] around $x = 0.46$ in the $Fe_xCo_{1-x}Ta_2O_6$ series. These changes are: (i) sign reversal of the nn interaction J_1, which is positive for x above 0.46 and negative below; (ii) sign change of the nnn interaction perpendicular to the anisotropy axis, J_2', which is positive for low x but becomes small and negative for $x > 0.46$; (iii) enhancement of the nnn interaction along the anisotropy axis, J_2, in the low x region (without changing its AF character). While $J_4 > 0$ favors the AFI phase, one needs $J_4 < 0$ and a fine tuning of J_3, J_3', and $|J_4|$ to account for the transition from AFI to AFC that occurs at very low Fe concentration ($x \sim 0.01$).

(iii) The AFN structure, with propagation vectors $(1/4, 1/4, 1/2)$, occurs for compositions with low Fe content in the $Fe_xNi_{1-x}Ta_2O_6$ series. Using magnetic susceptibility data from [12], we performed fittings with the high-temperature series presented in [10], obtaining the in-plane exchange constants $J_1 = -0.66$ K, $J_2 = -4.9$ K and $J_2' = 0.92$ K for $NiTa_2O_6$. The situation is very similar to the case of $CoTa_2O_6$ (see figure 3), with a maximum of $\lambda_{1+}^{pl}(k_a, k_b)$ for $k_a = k_b \equiv \kappa \simeq 0.52$, this value being given by (18). The stability of the AFN phase as a three-dimensional structure implies that the interplane couplings are such that $J_4 < 0$ and its absolute value is sufficiently large to fall outside the stability region of the AFC phase, given by (23).

The above comments imply that the exchange constant J_4 changes sign twice throughout the $Fe_xCo_{1-x}Ta_2O_6$ series, being negative for high or very low Fe content, and positive in the intermediate region $0.01 < x < 0.46$. Sign changes also occur near $x = 0.46$ for the in-plane exchange constants J_1 and J_2'. Similar changes must also occur in the $Fe_xNi_{1-x}Ta_2O_6$ series. To understand this, we have to keep in mind that we are dealing with magnetic ions at the center of distorted octahedra whose vertices are occupied by oxygen ions. Thus, we have what we could call generalized superexchange interactions, which in some cases are mediated by two or more of these oxygen ions, and could also involve the Ta cations. Only J_2 is associated with a straight-line superexchange path (see figure 1). All the others involve two or more bonds with relative angles far from 180°, in which case changes between AF and FM coupling usually occur [24–26]. As the magnetic-cation composition changes, the distortions of the surrounding octahedra are modified, which can lead to important intensity and sign variations of the exchange couplings.

It is worth remarking that one would not expect such a relevant role played by a longer range exchange coupling as J_4, while the shorter range J_3 is less effective. This behavior is tied to the existence of strong anisotropy with easy axes that are perpendicular to each other in adjacent planes. It is clear that a Heisenberg exchange interaction, depending on the scalar product of two spins, tends to be suppressed if an orthogonal relative orientation of these spins is favored by the anisotropy. In addition, we checked that a Dzyaloshinsky–Moriya interaction [27, 28] ($\mathbf{d}_{DM} \cdot \mathbf{S}_1 \times \mathbf{S}_2$) between nearest neighbors on adjacent planes would also be ineffective because, by symmetry reasons, the $\mathbf{d}_{DM}$ vector would be parallel to the planes containing the two easy axes.

4. Conclusions

We presented here the first three-dimensional model to describe magnetism in the tetragonal tantalite compounds $A_xA'_{1-x}Ta_2O_6$, mainly focusing on the $Fe_xCo_{1-x}Ta_2O_6$ series, for which extensive experimental investigations have been previously reported [5, 9, 10], but also with consistent results for $NiTa_2O_6$ [12, 13]. With this model, we obtained information about the possible magnetic structures by studying the maxima of the **k**-space exchange matrix, including single-ion anisotropy.

We were able to check the consistency of the possible magnetically ordered structures with the exchange constant values obtained from fittings of magnetic susceptibility data to high-temperature series for a two-dimensional model [10]. We confirmed that the stability of the solutions is intimately related to the existence of strong crystal-field anisotropy. We also verified the stability of the observed magnetic phases against weak interplane couplings, consistent with the quasi-two-dimensional nature of the magnetism in these compounds. Besides that, we were able to identify relevant relations between interplane interactions to account for the complete three-dimensional propagation vectors of the observed magnetic structures.

This analysis can be applied to other compounds in the general family AB_2O_6, like those with Nb [29, 30] or Sb [11, 31, 32] in place of Ta. While the model is directly applicable to the isostructural Sb compounds, a straightforward extension must be made in the case of Nb, for which the lattice structure is orthorhombic instead of tetragonal.

It is important to stress that the two-dimensional model alone could not account for the periodicities of the magnetic structure along the *c* axis observed in the tantalites, which depend exclusively on interplane coupling. The information we could gather here about interplane exchange constants was in good part qualitative, restricted to signs and orders of magnitude. More quantitative results may be achieved via different approaches. One alternative would be to develop the high-temperature series for the magnetic susceptibility using the fully three-dimensional model proposed here, followed by new fittings of the experimental data. A totally different line of investigation would involve *ab initio* calculations of the exchange integrals and crystal-field anisotropy, taking into account the actual chemical compositions within the unit cell. Due to the structural complexity of the compounds, both approaches are very difficult to pursue, but their results would be of great value for a broader and deeper understanding of the magnetic properties of these systems. We must also mention that detailed experimental data on spin-wave dispersion relations, as provided by inelastic neutron diffraction in single crystals, would also be suitable to extract information on exchange constants and anisotropy parameters with our model.

Acknowledgments

This work was supported in part by the French–Brazilian agreement CAPES-COFECUB and the Brazilian agency CNPq. Financial support of the Region Rhone-Alpes (France) via the ARCUS-Brésil cooperation program is also warmly acknowledged.

References

[1] Eicher S M, Greedan J E and Lushington K J 1986 *J. Solid State Chem.* **62** 220
[2] Zawislak L I, da Cunha J B M, Vasquez A and dos Santos C A 1995 *Solid State Commun.* **94** 345

[3] Zawislak L I, Fraga G L F, da Cunha J B M, Schimitt D, Carriço A S and dos Santos C A 1997 *J. Phys.: Condens. Matter* **9** 2295
[4] Antonietti V, Kinast E J, Zawislak L I, da Cunha J B M and dos Santos C A 2001 *J. Phys. Chem. Solids* **62** 1239
[5] Kinast E J, Antonietti V, Schmitt D, Isnard O, da Cunha J B M, Gusmão M A and dos Santos C A 2003 *Phys. Rev. Lett.* **91** 197208
[6] Kremer R K and Greedan J E 1988 *J. Solid State Chem.* **73** 579
[7] Kremer R K, Greedan J E, Gmelin E, Dai W, White M A, Eicher S M and Lushington K J 1988 *J. Physique* **49** 1495–6
[8] Reimers J N, Greedan J E, Stager C V and Kremer R 1989 *J. Solid State Chem.* **83** 20
[9] Kinast E J, dos Santos C A, Schmitt D, Isnard O, Gusmão M A and da Cunha J B M 2010 *J. Alloys Compounds* **491** 44
[10] Santos E G, de Oliveira Neto S R, Kinast E J, da Cunha J B M, Isnard O and Gusmão M A 2010 *J. Phys.: Condens. Matter* **22** 496004
[11] Ehrenberg H, Wltschek G, Rodriguez-Carvajal J and Vogt T 1988 *J. Magn. Magn. Mater.* **184** 111
[12] de Oliveira Neto S R, Kinast E J, Gusmão M A, dos Santos C A, Isnard O and da Cunha J B M 2007 *J. Phys.: Condens. Matter* **19** 356210
[13] Oliveira Neto S R, Kinast E J, Isnard O, da Cunha J B M, Gusmão M A and dos Santos C A 2008 *J. Magn. Magn. Mater.* **320** e125
[14] Muraoka Y, Idogaki T and Uryu N 1988 *J. Phys. Soc. Japan* **57** 1758
[15] Hague J P, Chung E M L, Visser D, Balakrishnan G, Clementyev E, Paul D M and Lees M R 2005 *J. Phys.: Condens. Matter* **17** 7227
[16] Villain J 1959 *J. Phys. Chem. Solids* **11** 303
[17] Kaplan T A 1960 *Phys. Rev.* **119** 1460
[18] Lyons D H and Kaplan T A 1960 *Phys. Rev.* **120** 1580
[19] Freiser M J 1961 *Phys. Rev.* **123** 2003
[20] Lyons D H, Kaplan T A, Dwight K and Menyuk N 1962 *Phys. Rev.* **126** 540
[21] Bertaut E F 1961 *J. Phys. Chem. Solids* **21** 256
[22] Bertaut E F 1961 *J. Phys. Chem. Solids* **21** 295
[23] Bak P 1982 *Rep. Prog. Phys.* **45** 587
[24] Goodenough J B 1958 *J. Phys. Chem. Solids* **6** 287
[25] Goodenough J B 1963 *Magnetism and the Chemical Bond* (New York: Interscience–Wiley)
[26] Kanamori J 1959 *J. Phys. Chem. Solids* **10** 87
[27] Dzyaloshinsky I 1958 *J. Phys. Chem. Solids* **4** 241
[28] Moriya T 1960 *Phys. Rev.* **120** 91
[29] Heid C, Weitzel H, Burlet P, Bonnet M, Gonschorek W, Vogt T, Norwig J and Fuess H 1995 *J. Magn. Magn. Mater.* **151** 123
[30] Pullar R C 2009 *J. Am. Ceram. Soc.* **92** 563
[31] Reimers J, Greedan J E, Stager C V and Kremer R 1989 *J. Solid State Chem.* **83** 20
[32] Kato M, Tomohiko I, Kajimoto K, Yoshimura K, Kosuge K, Nishi M and Kakurai K 2002 *J. Phys. Chem. Solids* **63** 1129